Analytic and Numerical Studies of a Simple Model of Attractive-Repulsive Swarms

Andrew S. Ronan

Andrew J. Bernoff, Advisor

Chad M. Topaz, Reader

May, 2011

HARVEY MUDD COLLEGE

Department of Mathematics

Copyright © 2011 Andrew S. Ronan.

The author grants Harvey Mudd College and the Claremont Colleges Library the nonexclusive right to make this work available for noncommercial, educational purposes, provided that this copyright statement appears on the reproduced materials and notice is given that the copying is by permission of the author. To disseminate otherwise or to republish requires written permission from the author.

The author is also making this work available under a Creative Commons Attribution–NonCommercial–ShareAlike license.

See http://creativecommons.org/licenses/by-nc-sa/3.0/ for a summary of the rights given, withheld, and reserved by this license and http://creativecommons.org/licenses/by-nc-sa/3.0/legalcode for the full legal details.

Abstract

We study the equilibrium solutions of an integrodifferential equation used to model one-dimensional biological swarms. We assume that the motion of the swarm is governed by pairwise interactions, or a convolution in the continuous setting, and derive a continuous model from conservation laws. The steady-state solution found for the model is compactly supported and is shown to be an attractive equilibrium solution via linear perturbation theory. Numerical simulations support that the steady-state solution is attractive for all initial swarm distributions. Some initial results for the model in higher dimensions are also presented.

Contents

Abstract iii

Acknowledgments ix

1 Introduction 1
- 1.1 Literature Review . . . 2

2 Mathematical Formulation of the Model 5
- 2.1 Discrete Model . . . 5
- 2.2 Continuous Model . . . 6
- 2.3 Properties of the Model . . . 8

3 Steady-State Solution and Energy Minimization 9
- 3.1 Steady-State Solution . . . 10
- 3.2 Energy Functional . . . 11
- 3.3 Perturbations Inside Support . . . 13
- 3.4 Perturbations Outside Support . . . 16
- 3.5 Linear Perturbations . . . 17

4 Extensions to Higher Dimensions 21
- 4.1 The Model in Higher Dimensions . . . 21
- 4.2 Solution Intervals and Nonphysical Solutions . . . 23

5 Numerical Simulations 27
- 5.1 Derivation of the Model . . . 27
- 5.2 Analysis . . . 28
- 5.3 Numerical Simulations in Higher Dimensions . . . 31

6 Conclusions and Future Work 35

Bibliography **37**

List of Figures

3.1 Eigenfunction corresponding to the minimum eigenvalue in the linear perturbation equations 19

4.1 Physical solutions to the eigenvalue problem in $\mathbb{R}^3$ 24
4.2 A steady-state solution in three dimensions and a physical steady-state solution for a confined interval 25

5.1 Particle simulation positions and error over time 29
5.2 Natural log of L_2 error over time 30
5.3 Particle method point wise error 31
5.4 Comparison of the numerical and analytical eigenfunctions 32
5.5 Particle simulation in three dimensions compared to a non-linear least squares fit of the analytical solutions 34

Acknowledgments

I would like to thank my research advisor, Andrew Bernoff, for his immense patience, advice, and support.

Chapter 1

Introduction

Many biological species, including insects, and fish, behave as swarms and form groups or aggregations naturally. This behavior is motivated by endogenous social interactions as well as exogenous factors. Endogenous interactions can arise because organisms sense each other through a variety of different methods including sight, touch, smell, chemical interactions, and vibrations. These interactions can result in attractive or repulsive forces between the organisms. For example, while some organisms may group together for safety, they will not concentrate to the point of stacking on top of each other. The endogenous interactions may be coupled with exogenous forces such as wind or gravity via superposition to account for the forces acting on the entire swarm. These forces can lead to a variety of different swarm shapes or equilibrium solutions. For examples, see Bernoff and Topaz (2010); Bodnar and Velazquez (2005, 2006); Leverentz, Topaz, and Bernoff (2009); Mogilner, Edelstein-Keshet, Bent, and Spiros (2003).

Different models of swarming behavior may choose to incorporate different forces, and may model them in a variety of ways. In addition, the model may be continuous or discrete. Discrete models, which are more easily relatable to biological swarms, represent each organism as a particle with a position and velocity based on the locations of the other organisms (Mogilner et al., 2003). Typically, the organisms are modeled as interacting in a pairwise manner so that each organism's velocity is based on the sum of the pairwise and exogenous forces. Continuous models instead describe the swarm in terms of a continuous-density function or cumulative-density function where the velocity of the swarm at a particular point is based on a convolution over the swarm that represents the continuous analog of pairwise interactions.

In this thesis, I examine a particular continuous model that contains attractive and repulsive interaction forces with no exogenous forces acting on the swarm. I consider a one-dimensional model where the velocity at a point is directly proportional to the net social force felt at that point. The density of the swarm for a given position and time is governed by the following integrodifferential equation:

$$\rho_t + (\rho V)_x = (\rho \rho_x)_x, \tag{1.1}$$

$$V(x,t) = \int_{\infty}^{\infty} \rho(z,t)\text{sgn}(x-z)\, dz. \tag{1.2}$$

The density is denoted by $\rho(x,t)$ at a position x and time t. The attractive-velocity component, $V(x,t)$, is a convolution of the signum function with the density. Finally, the $(\rho\rho_x)_x$ term is the porous-medium regularization of the repulsive component of the endogenous interactions, which is where the distance of the repulsive component is arbitrarily small. For more information on this limiting case, see Bodnar and Velazquez (2006).

1.1 Literature Review

Early work on modeling particle interactions was done by Mogilner and colleagues (2003). They formulate a Lagrangian model to examine the spacing of members of a discrete swarm using pairwise interactions between all members of the group to model interactions. In addition, Mogilner and his colleagues find conditions on the choices of attractive and repulsive functions such that the function does not blow up.

Others, such as Bodnar and Velazquez (2006; 2005), Bernoff and Topaz (2010), and Leverentz and colleagues (2008; 2009), have studied many variations of a more general one-dimensional continuous model given by

$$\rho_t + (\rho v)_x = 0 \tag{1.3}$$

$$v(x) = \int_{\mathbb{R}} q(x-y)\rho(y)\, dy + f(x), \tag{1.4}$$

where $v(x)$ is a velocity field, $q(z)$ is the pairwise endogenous force, and $f(x)$ represents any exogenous forces. For an antisymmetric endogenous force $q(z)$, this model displays at least three different solution types that the density distribution can converge to. Populations can concentrate to a delta function at a point, spread out infinitely, or reach a finite steady-state.

Bodnar and Velazquez (2005) derive the continuous governing Equation 1.3 from a discrete model. They explore conditions for well-posedness as well as finite time blow up for Equation 1.3. In addition, they also examine possible steady-state solutions and show that some may exhibit more complicated structure than finite-time blowup or infinite spreading. Bodnar and Velazquez (2006) examine the change in density over time with the addition of a stochastic element.

Bedrossian and colleagues (2010) examine higher-dimensional aggregation equations with degenerate diffusion. For the set of equations they examine they determine a critical mass such that for initial solutions with masses greater than the critical mass there is finite time blow up, whereas for solutions with less initial mass there is global existence. This is similar to the work of Bertozzi and Slepcev (2010), which proves existence and uniqueness of weak solutions to the same general equation but with a non-singular attractive kernel.

Bernoff and Topaz (2010) examine a two-dimensional model for locust swarming. Additionally, they look at one-dimensional swarming models from an energy minimization and calculus of variations perspective to determine some conditions for steady-state solutions. The approach taken in this thesis is similar to that taken by Bernoff and Topaz as well as Leverentz (2008); however, the analysis is conducted only on a particular one-dimensional model.

Brecht and colleagues (2011) determine how different combinations of attractive and repulsive forces change energy minimizers on the surface of a sphere by solving an eigenvalue problem in three dimensions. Interestingly, although for some parameter choices the distributions have radial symmetry, there are a number of energy minimizers with much more complex forms. Huang and Bertozzi (2010) also examine the same continuous model in $\mathbb{R}^n$, but instead examine conditions under which there the density blows up at some point. Their approach is very similar to the eigenvalue problem examined in Chapter 4.

Chapter 2

Mathematical Formulation of the Model

In this chapter I will define the discrete particle interaction model and then derive the continuum model from the discrete model. I will demonstrate that the center of mass remains unchanged, which will be important when examining perturbations from the steady-state solution in Chapter 3.

2.1 Discrete Model

For the discrete model, consider N identical particles in one spatial dimension with positions given by x_i. These particles may represent biological organisms engaged in swarming. By assuming that the motion of the particles is governed by Newton's law, the acceleration is proportional to the force acting on the particle. We will use a kinetic model where the acceleration is negligible and, as a result, drag force is directly proportional to the motive force or velocity of the particle. For a more in-depth discussion of this approach, see Bernoff and Topaz (2010).

To simplify the model we assume that the endogenous forces act in an additive pairwise manner and that the force is antisymmetric. In addition, we will disregard any exogenous forces acting on the particles and consider only endogenous forces. Thus the force from particle i felt by particle j is the opposite of the force from particle j felt by particle i and there are no other effects such as wind or gravity.

Given these assumptions, the governing equation for the discrete model takes the form

$$\frac{dx_i}{dt} = V_i(x_1, \ldots, x_N), \tag{2.1}$$

$$V_i(x_1, \ldots, x_N) = \sum_{\substack{j=1 \\ j \neq i}}^{N} mq(x_i - x_j), \qquad m = M/N. \tag{2.2}$$

Here M is the total mass of the swarm and q is the antisymmetric endogenous force of one particle on another. The mass of each δ-function, m, is defined so that as the number of particles increases the mass remains constant.

2.2 Continuous Model

In order to derive a continuum model, we describe the set of particles in the discrete model as δ-functions of size m. Then the density at a point x is the sum of the δ-functions. Therefore,

$$\rho(x) = \sum_{i=1}^{N} m\delta(x - x_i), \tag{2.3}$$

and the total mass is

$$M = \int_{-\infty}^{\infty} \rho(x)\, dx = mN. \tag{2.4}$$

In addition, we can rewrite the discrete velocity for a point x as

$$v(x) = \int_{-\infty}^{\infty} q(x - y)\rho(y)\, dy. \tag{2.5}$$

Here the summation is replaced by a convolution, but q remains the same. The mass for a given region of the swarm is

$$M = \int_a^b \rho(x, t) dx, \tag{2.6}$$

where the flux Q in the region is given by

$$Q = \rho(a)v(a) - \rho(b)v(b). \tag{2.7}$$

Then, by conservation of mass and the fundamental theorem of calculus, we can rewrite Equation 2.7 as

$$\frac{dM}{dt} = Q = -\int_a^b (\rho(x)V(x))_x dx \tag{2.8}$$

Taking a time derivative of the mass equation, equating Equation 2.6 with Equation 2.8, and rearranging terms,

$$\int_a^b \rho_t + (\rho v)_x \, dx = 0. \tag{2.9}$$

Equation 2.9 holds for any interval $[a, b]$, so

$$\rho_t + (\rho v)_x = 0. \tag{2.10}$$

For our model, the velocity term V can be represented as a combination of attractive and repulsive velocities, where

$$v(x) = v_a(x) + v_r(x). \tag{2.11}$$

The attractive component is chosen as

$$v_a(x) = \int_{-\infty}^{\infty} \rho(y)\mathrm{sgn}(x - y) \, dy, \tag{2.12}$$

so that the attractive component of a point's velocity is independent of distance and dependent only on the amount of mass to the left and right on the real axis. Next, for the repulsive force we want a force that is highly repulsive at short distances, negligible at larger distances, and never attractive. In order to accomplish these force requirements, let

$$F_r(x) = q(x), \tag{2.13}$$

where q is odd and $xq > 0$ for $x > 0$. Let ϵ represent the approximate size of the region where the force is repulsive, and let q be near zero elsewhere. Then

$$v_r(x) = \int_{-\infty}^{\infty} \rho(y)q(x - y) \, dy = \int_{-\infty}^{\infty} \rho(x - y)q(y) \, dy. \tag{2.14}$$

Taylor expanding $\rho(x - y)$ and substituting the result back into the repulsive velocity function, we get

$$v_r(x) = -\rho_x(x)C\epsilon^2 + \mathcal{O}(\epsilon^4), \tag{2.15}$$

where C is a constant. The y variables from the Taylor expansion have been replaced by epsilon because $q(y) \approx 0$ outside of a distance of ϵ away from y. Substituting v_r and v_a into the governing equation we derive our original model

$$\rho_t + (\rho V)_x = (\rho\rho_x)_x \tag{2.16}$$

$$V(x, t) = \int_{-\infty}^{\infty} \rho(z, t)\mathrm{sgn}(x - z) \, dz, \tag{2.17}$$

where V represents the attractive component.

2.3 Properties of the Model

By virtue of the derivation of the governing equation, the model observes conservation of mass for any swarm of finite mass. The antisymmetry of the endogenous forces in the model leads to interactions between each component of the swarm in equal magnitude and opposite direction. The lack of exogenous forces implies that the center of mass of the system should remain constant. Since this should hold for all antisymmetric endogenous forces for simplicity and generality, we will derive this fact for the general model

$$\rho_t + (\rho v)_x = 0, \tag{2.18}$$

mentioned before, where there are only endogenous forces. For a more complete derivation, see Leverentz (2008).

Consider the center of mass at time t,

$$\bar{x}(t) = \frac{1}{M}\int_{-\infty}^{\infty} x\rho(x,t)\,dx. \tag{2.19}$$

Then, taking a time derivative of both sides, substituting from the governing equation, and applying the chain rule,

$$\begin{aligned}
\frac{d\bar{x}}{dt} &= \frac{1}{M}\int_{-\infty}^{\infty} x\rho_t\,dx && (2.20)\\
&= -\frac{1}{M}\int_{-\infty}^{\infty} x(\rho v)_x\,dx && (2.21)\\
&= -\frac{1}{M}x\rho v|_{x=-\infty}^{x=\infty} + \frac{1}{M}\int_{-\infty}^{\infty} \rho v\,dx. && (2.22)
\end{aligned}$$

For a finite mass the density vanishes at ±∞, thus

$$\frac{d\bar{x}}{dt} = \frac{1}{M}\int_{-\infty}^{\infty}\int_{-\infty}^{\infty} \rho(x,t)\rho(y,t)q(x-y)\,dy\,dx, \tag{2.23}$$

where $q(x)$ represents the pairwise endogenous forces. By relabeling the variables of integration and invoking the antisymmetry of the endogenous forces, it follows that

$$\frac{d\bar{x}}{dt} = -\frac{d\bar{x}}{dt} = 0. \tag{2.24}$$

Therefore, the center of mass remains unchanged for any finite swarm distribution.

Chapter 3

Steady-State Solution and Energy Minimization

In this chapter I will derive the steady-state solution via two different approaches. Initial results of an energy minimization argument demonstrating global convergence to the steady-state solution is shown along with results from linear perturbation theory that indicate convergence.

Consider the cumulative density function defined by

$$\psi(x) = \int_{-\infty}^{x} \rho(s)\, ds. \tag{3.1}$$

Assuming continuity of ρ, then $\psi_x = \rho$. Substituting $\psi(x)$ into the governing equation,

$$(\psi_t)_x + ((M - 2\psi)\psi_x)_x = (\psi_x \psi_{xx})_x, \tag{3.2}$$

because

$$\begin{aligned} V(x) &= -\int_{-\infty}^{x} \rho(y)\, dy + \int_{x}^{\infty} \rho(y)\, dy && (3.3)\\ &= -\psi_x + M - \psi_x && (3.4)\\ &= M - 2\psi_x. && (3.5) \end{aligned}$$

Next, integrating both sides of the governing equation, we get a partial differential equation in terms of ψ given by

$$\psi_t + (M - 2\psi)\psi_x = \psi_x \psi_{xx}. \tag{3.6}$$

Here $\lim_{x\to-\infty} \psi(x) = 0$ and $\lim_{x\to\infty} \psi(x) = M$ where M is the total mass of the swarm.

3.1 Steady-State Solution

By setting the ψ_t term of the governing equation to 0, we obtain an ordinary differential equation in terms of x that can be solved to find the steady-state solution. The differential equation is

$$(M - 2\psi)\psi_x = \psi_x \psi_{xx}. \tag{3.7}$$

Outside the support of the solution $\psi_x = \rho = 0$. Inside the support by definition $\psi_x \neq 0$. From these assumptions we can simplify the ODE further to

$$\psi_{xx} + 2\psi = M. \tag{3.8}$$

Because the solution is translationally invariant, a steady-state solution is given by

$$\psi(x) = \begin{cases} 0 & x \leq \frac{-\pi}{2\sqrt{2}}, \\ \frac{M}{2}\sin(\sqrt{2}x) + \frac{M}{2} & -\frac{\pi}{2\sqrt{2}} \leq x \leq \frac{\pi}{2\sqrt{2}}, \\ M & x \geq \frac{-\pi}{2\sqrt{2}}. \end{cases} \tag{3.9}$$

Differentiating $\psi(x)$ we obtain the the steady-state solution for the density function,

$$\rho(x) = \begin{cases} 0 & x \leq \frac{-\pi}{2\sqrt{2}}, \\ \frac{\sqrt{2}M}{2}\cos(\sqrt{2}x) & -\frac{\pi}{2\sqrt{2}} \leq x \leq \frac{\pi}{2\sqrt{2}}, \\ 0 & x \geq \frac{-\pi}{2\sqrt{2}}. \end{cases} \tag{3.10}$$

Alternatively, we can consider the mutual-interaction potential, $Q(z)$ defined by

$$Q(z) = \int^{z} q(s)\, ds. \tag{3.11}$$

Then, by definition of the total velocity, it follows that

$$v(x) = -[Q * \rho]_x. \tag{3.12}$$

For the specific choice of velocity we have, then

$$Q(z) = \delta(z) + |z|. \tag{3.13}$$

Consider a steady-state solution, $\bar{\rho}$, then $v(x) = 0$ when the density is given by $\bar{\rho}(x)$. Therefore from Equation 3.12, we have

$$0 = -[Q * \bar{\rho}]_x. \tag{3.14}$$

Integrating both sides with respect to x,

$$\lambda = -Q * \bar{\rho} \tag{3.15}$$

for some constant λ. Substituting in $Q(z) = \delta(z) + |z|$ and absorbing the negative sign into the constant yields the integral equation

$$\begin{aligned} \lambda &= \int_{-\infty}^{\infty} \bar{\rho}(y)(\delta(x-y) + |x-y|)\, dy && (3.16) \\ &= \bar{\rho}(x) + \int_{-\infty}^{\infty} \bar{\rho}(y)|x-y|\, dy. && (3.17) \end{aligned}$$

Applying the operator ∂_{xx} to Equation 3.16 yields the differential equation

$$0 = \bar{\rho}_{xx} + 2\bar{\rho}. \tag{3.18}$$

Because the system is translationally invariant, has finite mass, and must satisfy the initial integral equation, the solution for $\bar{\rho}$ is identical to Equation 3.10.

3.2 Energy Functional

The total energy or energy potential of a swarm configuration is given by

$$W[\rho] = \frac{1}{2} \int_\Omega \int_\Omega \rho(x)\rho(y)Q(x-y)\, dx\, dy. \tag{3.19}$$

The energy potential is analogous to the discrete potential, which is one half of a double sum over all the points in order to discount the double counting. For a more in-depth discussion of the energy potential, see Bernoff and Topaz (2010) where the energy functional is derived from the discrete potential.

In addition, the rate of energy dissipation is given by

$$\frac{dW[\rho]}{dt} = -\int_\Omega \rho(x)v(x)^2\, dx, \tag{3.20}$$

where $v(x)$ is the sum of the attractive and repulsive components of the velocity. The derivation is as follows,

$$\begin{aligned} \frac{dW[\rho]}{dt} &= \frac{d}{dt}\frac{1}{2} \int_\Omega \int_\Omega \rho(x)\rho(y)Q(x-y)\, dx\, dy && (3.21) \\ &= \int_\Omega \int_\Omega \rho(x)_t \rho(y)Q(x-y)\, dx\, dy. && (3.22) \end{aligned}$$

Equation 3.21 follow from the product rule and symmetry of $\rho(x)$ and $\rho(y)$. Then, substituting in from the general governing equation and rewriting the second integral as a convolution,

$$\frac{dW[\rho]}{dt} = -\int_{\Omega} (v\rho)_x[x](Q*\rho)[x]\, dx. \tag{3.23}$$

Integrating by parts and substituting in Equation 3.12, Equation 3.21 becomes

$$\frac{dW[\rho]}{dt} = -\int_{\Omega} (v\rho)[x](Q*\rho)_x[x]\, dx. = -\int_{\Omega} \rho(x)v(x)^2\, dx. \tag{3.24}$$

Thus the change in energy is always less than or equal to zero. In addition, there is no change in energy at points with no density. Therefore, if a solution has reached an energy minimum then it is an attractive equilibrium solution with some basin of attraction.

We examine perturbations from the steady-state solution to determine under what conditions or perturbations it is a minimizer of the total energy W. Consider a swarm configuration given by

$$\rho(x) = \bar{\rho} + \tilde{\rho}(x). \tag{3.25}$$

Here $\bar{\rho}$ is the steady-state solution and $\tilde{\rho}$ is a zero-mass perturbation. Thus if $\bar{\rho}$ is a steady-state solution of mass M then

$$\int_{\Omega} \bar{\rho}(x)\, dx = M, \tag{3.26}$$

$$\int_{\Omega} \tilde{\rho}(x)\, dx = 0. \tag{3.27}$$

In addition, because the solutions are translationally invariant and the center of mass is maintained we only need consider perturbations that do not change the center of mass. Thus

$$\int_{\Omega} x\tilde{\rho}(x)\, dx = 0. \tag{3.28}$$

Because W is quadratic in ρ, the energy of the configuration with a perturbation is given by

$$W[\rho] = W[\bar{\rho}] + 2W_1[\bar{\rho}, \tilde{\rho}] + W_2[\tilde{\rho}, \tilde{\rho}], \tag{3.29}$$

where W_1 and W_2 are the first and second variations, respectively.

3.3 Perturbations Inside Support

Consider a perturbation of the form $\rho(x) = \bar{\rho} + \tilde{\rho}(x)$ where the support of $\tilde{\rho}(x)$ lies inside the region of support of $\bar{\rho}$. The difference in the energies of $W[\bar{\rho}]$ and $W[\rho]$ is

$$\Delta W = 2W_1[\bar{\rho}, \tilde{\rho}] + W_2[\tilde{\rho}, \tilde{\rho}]. \tag{3.30}$$

First, let us define

$$\Lambda(x) = Q * \bar{\rho}. \tag{3.31}$$

Then, differentiating with respect to x, we get

$$\Lambda(x)_x = [Q * \bar{\rho}]_x = V(x) \tag{3.32}$$

from Equation 3.12. If we are only concerned with the region where x is in the support of $\bar{\rho}$, then $V(x) = 0$. As a result,

$$\Lambda(x) = \lambda \tag{3.33}$$

in the support of $\bar{\rho}$.

The first variation is given by

$$\begin{aligned}
W_1[\bar{\rho}, \tilde{\rho}] &= \int_\Omega \int_\Omega \tilde{\rho}(x)\bar{\rho}(y)Q(x-y)\, dy\, dx & (3.34)\\
&= \int_\Omega \tilde{\rho}(x)[\int_\Omega \bar{\rho}(y)Q(x-y)\, dy]\, dx & (3.35)\\
&= \int_\Omega \tilde{\rho}(x)\Lambda(x)\, dx. & (3.36)
\end{aligned}$$

Because we are integrating over the support of $\bar{\rho}$, it follows from Equation 3.33 that

$$\begin{aligned}
W_1[\bar{\rho}, \tilde{\rho}] &= \int_\Omega \tilde{\rho}(x)\Lambda(x)\, dx & (3.37)\\
&= \lambda \int_\Omega \tilde{\rho}(x)\, dx & (3.38)\\
&= 0. & (3.39)
\end{aligned}$$

By the zero-mass constraint on $\tilde{\rho}$. Therefore, the change in energy for perturbations inside the support of $\bar{\rho}$ is

$$\Delta W = W_2[\tilde{\rho}, \tilde{\rho}] = \frac{1}{2} \int_\Omega \int_\Omega \tilde{\rho}(x)\tilde{\rho}(y)Q(x-y)\, dy\, dx. \tag{3.40}$$

Next, we examine the Fourier transform of Q to analyze ΔW. Define the Fourier transform

$$\hat{Q}(k) = \int_{-\infty}^{\infty} Q(x)e^{-ikx}\,dx. \tag{3.41}$$

Then

$$\begin{aligned} W_2[\tilde{\rho},\tilde{\rho}] &= \frac{1}{2}\int_\Omega \int_\Omega \tilde{\rho}(x)\tilde{\rho}(y)Q(x-y)\,dy\,dx & (3.42)\\ &= \frac{1}{2}\int_{-\infty}^{\infty}\int_{-\infty}^{\infty} \tilde{\rho}(x)\tilde{\rho}(y)Q(x-y)\,dy\,dx & (3.43)\\ &= \frac{1}{2}\int_{-\infty}^{\infty} \tilde{\rho}(x)[\tilde{\rho}(x) * Q(x)]\,dx & (3.44)\\ &= \frac{1}{4\pi}\int_{-\infty}^{\infty} |\hat{\tilde{\rho}}(k)|^2\hat{Q}(k)\,dk, & (3.45) \end{aligned}$$

where we have used the fact that $\tilde{\rho}$ is real, and compactly supported as well as the convolution theorem and Parseval's Theorem. For the set of endogenous forces in our model,

$$\hat{Q}(k) = 1 - \frac{2}{|k|^2}. \tag{3.46}$$

Because $\hat{Q}(k)$ is not necessarily greater than zero, we analyze the eigenvalue problem.

A necessary and sufficient condition for $W_2 > 0$ comes from considering the spectrum of I in Ω, where

$$W_2[\tilde{\rho},\tilde{\rho}] = \int_\Omega I[\tilde{\rho}]\tilde{\rho}(x)dx. \tag{3.47}$$

Assuming the perturbation is nontrivial, then if the eigenvalues of I are positive it follows that $W_2 > 0$. Define μ_n such that for ρ_n,

$$\mu_n\rho_n(x) = \int_\Omega \rho_n(y)Q(x-y)\,dy. \tag{3.48}$$

Then, substituting in Q, we have

$$\begin{aligned} \mu_n\rho_n(x) &= \int_\Omega \rho_n(y)(|x-y| + \delta(x-y))\,dy & (3.49)\\ &= \rho_n(x) + \int_\Omega \rho_n(y)|x-y|\,dy. & (3.50) \end{aligned}$$

Because $\int_\Omega \rho(y)\delta(x-y)\,dy = \rho(x)$. Applying the differential operator $\frac{d^2}{dx^2}$ to eigenvalue problem yields the differential equation

$$(\mu_n - 1)\rho_n''(x) = 2\rho_n(x). \tag{3.51}$$

When $\mu_n > 1$, solutions are of the form of exponentials; however, when $\mu_n < 1$, solutions to the integral equation have the form

$$\rho_n = C_1 \cos\sqrt{\frac{2}{1-\mu_n}}x + C_2 \sin\sqrt{\frac{2}{1-\mu_n}}x. \tag{3.52}$$

Here C_1 and C_2 are constants of integration. Therefore the possible eigenfunctions are

$$\mu_{n_{odd}} = \sin\sqrt{\frac{2}{1-\mu_n}}x, \qquad \mu_{n_{even}} = \cos\sqrt{\frac{2}{1-\mu_n}}x. \tag{3.53}$$

For simplicity, let $a = \sqrt{\frac{2}{1-\mu_n}}$ and $l = \frac{\pi}{2\sqrt{2}}$. Then by plugging $\mu_{n_{odd}}$ back into the integral equation over the region of support of the steady-state solution, $[-l, l]$, the solution is

$$\mu_n \sin ax = \frac{2x\cos(al)}{a} + \frac{(a^2-2)\sin ax}{a^2}. \tag{3.54}$$

We constrain the possible values of μ_n so that there is no linear term. Thus

$$\frac{2x\cos(al)}{a} = 0. \tag{3.55}$$

As a result, the eigenvalues must be of the form

$$\mu_n = 1 - \frac{1}{(2k+1)^2}, \qquad k \in \mathbb{Z}. \tag{3.56}$$

When $k = 0$, the eigenvalue is zero, whereas for all other values of k the value of μ_n is in the range (0,1).

Next, using the same approach as for the odd eigenvalues, we substitute $\mu_{n_{even}}$ into the original integral equation. This yields

$$\mu_n \cos(ax) = \frac{(a^2-2)cos(ax)}{a^2} + \frac{2\cos(al) + 2al\sin(al)}{a^2}. \tag{3.57}$$

Again, we require that the constant term is zero. For this set of eigenfunctions, then,

$$\frac{2\cos(al) + 2al\sin(al)}{a^2} = 0, \tag{3.58}$$

or rearranging terms,

$$al = -\cot(al). \tag{3.59}$$

In terms of μ_n, Equation 3.59 requires that

$$\frac{\pi}{2}\sqrt{\frac{1}{1-\mu_n}} = -\cot\frac{\pi}{2}\sqrt{\frac{1}{1-\mu_n}}. \tag{3.60}$$

There are no negative eigenvalues that satisfy this constraint but, as in the case with the even eigenvalues, an infinite number in the interval $(0, 1)$. Because we also require that the perturbations satisfy Equation 3.27 and Equation 3.28, there are no even or odd eigenfunctions that satisfy this alone. Therefore we need to look for a combination of eigenfunctions to satisfy the physical constraints placed on the perturbation. As a result, we can disregard $\mu_n = 0$ as a possible eigenvalue for a perturbation because it does not satisfy Equation 3.28 alone.

Because there are no negative or zero eigenvalues, the steady-state solution is an energy minimizer for perturbations inside the support of the steady-state solution. While there are only positive eigenvalues, further work needs to be done to determine what is the smallest positive eigenvalue that meets the physical constraints of the problem as well as satisfies the eigenvalue problem. Finding the minimum of the Rayleigh quotient,

$$R(\tilde{\rho}) = \frac{W(\tilde{\rho}, \tilde{\rho})}{||\tilde{\rho}||^2} = \frac{\sum a_n^2 ||\tilde{\rho}||^2 \mu_n}{\sum a_n^2 ||\tilde{\rho}||^2}, \tag{3.61}$$

subject to the constraints Equation 3.27, Equation 3.28, and

$$||\tilde{\rho}||^2 \neq 0, \tag{3.62}$$

should yield a minimum eigenvalue. Unfortunately, there does not appear to be a finite number of eigenfunctions that when composed to make up $\tilde{\rho}$ satisfy the constraints.

3.4 Perturbations Outside Support

Next we can consider perturbations such that $\tilde{\rho} > 0$ outside the support of $\bar{\rho}$. From Bernoff and Topaz (2010), it suffices for $W_2 > 0$ to guarantee that $\bar{\rho}$ is a global minimizer. Because $\hat{Q}(k) > 0$, again we need to solve the eigenvalue problem for this extended region of support. Unfortunately this requires a similar approach to that of perturbations inside of the support. As a result, it is still an open question as to whether the eigenvalues of this problem are all strictly greater than zero. While the perturbation method leads to only some partial results, a similar approach from linear perturbation theory provides more insight.

3.5 Linear Perturbations

In order to linearize the problem, we again look at perturbations from the steady-state given by

$$\rho = \bar{\rho} + \epsilon\tilde{\rho}, \tag{3.63}$$

where $\bar{\rho}$ is the steady-state solution and $\epsilon\tilde{\rho}$ is a perturbation. We define the perturbation so that we can rewrite $\tilde{\rho}$ in the form

$$\tilde{\rho} = e^{\lambda t}\rho_0(x), \tag{3.64}$$

where $\rho_0(x)$ is some initial distribution in order to eventually derive an eigenvalue equation. The assumption about the time dependence of the perturbation holds in the limit as the perturbation becomes small and t gets large because the solution will decay to the steady-state solution at the rate of the dominant eigenvalue. The analysis becomes simpler, however, when looking at linear perturbations from the cumulative density function. Let

$$\psi = \bar{\psi} + \epsilon\tilde{\psi}, \tag{3.65}$$

where $\bar{\psi}$ is the steady-state solution and $\epsilon\tilde{\psi}$ is a perturbation. Again,

$$\tilde{\psi} = \tilde{\psi}_0(x)e^{\lambda t}, \tag{3.66}$$

where $\tilde{\psi}_0(x)$ is some initial distribution. The governing equation in terms of ψ, Equation 3.6, is

$$\psi_t + (M - 2\psi)\psi_x = \psi_x\psi_{xx}. \tag{3.67}$$

Substituting in $\psi = \bar{\psi} + \epsilon\tilde{\psi}$ into Equation 3.6 and separating the $\mathcal{O}(1)$ and order $\mathcal{O}(\epsilon)$ terms yields the system of equations

$$(M - 2\bar{\psi})\bar{\psi}_x = \bar{\psi}_x\bar{\psi}_{xx} \qquad \mathcal{O}(1), \tag{3.68}$$
$$\lambda\tilde{\psi} = (2\tilde{\psi} - \tilde{\psi}_{xx})\bar{\psi}_x \qquad \mathcal{O}(\epsilon). \tag{3.69}$$

Higher order terms in epsilon, in this case $\mathcal{O}(\epsilon^2)$, are ignored. The first equation in the system is the steady-state equation which is solved in Section 3.1, while the second equation is the linearized eigenvalue problem. Substituting in $\bar{\psi}_x$, the equation becomes

$$\lambda\tilde{\psi} = (2\tilde{\psi} - \tilde{\psi}_{xx})\frac{\sqrt{2}M}{2}\cos(\sqrt{2}x), \qquad -\frac{\pi}{2\sqrt{2}} \leq x \leq \frac{\pi}{2\sqrt{2}}. \tag{3.70}$$

Rearranging terms, the differential equation can be written as

$$\tilde{\psi}_{xx} = \left(2 - \frac{2\lambda}{\sqrt{2}M\cos(\sqrt{2}x)}\right)\tilde{\psi}. \tag{3.71}$$

At the boundaries of the solution when

$$x = -\frac{\pi}{2\sqrt{2}}, \quad x = \frac{\pi}{2\sqrt{2}}, \tag{3.72}$$

the coefficient on $\tilde{\psi}$ is not analytic. In order to simplify the following analysis, we will shift the solution over and remove the scaling on the sinusoidal term because the behavior remains the same regardless of how the coefficient is scaled. Then we can analyze the following equation,

$$u_{xx} = \left(2 - \frac{\lambda}{c\sin(x)}\right)u \tag{3.73}$$

The Laurent series expansion for $1/\sin(x)$ allows us to rewrite this as

$$u_{xx} = \left(2 - \frac{\lambda}{c}\right)\left[\frac{1}{x} + \frac{x}{6} + \frac{7x^3}{360} + \mathcal{O}(x^5)\right]u. \tag{3.74}$$

By the method of Frobenius, we can consider a solution of the form $u(x) = \sum_{k=0}^{\infty} C_k x^{k+\beta}$. Substituting in $u = x^\beta$,

$$\beta(\beta-1)x^{\beta-2} = \left(2 - \frac{\lambda}{c}\left[\frac{1}{x} + \frac{x}{6} + \frac{7x^3}{360} + \mathcal{O}(x^5)\right]\right)x^\beta. \tag{3.75}$$

In order for this to hold, we require that $\beta \geq 1$. As a result, $u(0) = 0$. Therefore, for eigenvalue problem we require that the following boundary conditions hold,

$$\tilde{\psi}\left(-\frac{\pi}{2\sqrt{2}}\right) = \tilde{\psi}\left(\frac{\pi}{2\sqrt{2}}\right) = 0 \tag{3.76}$$

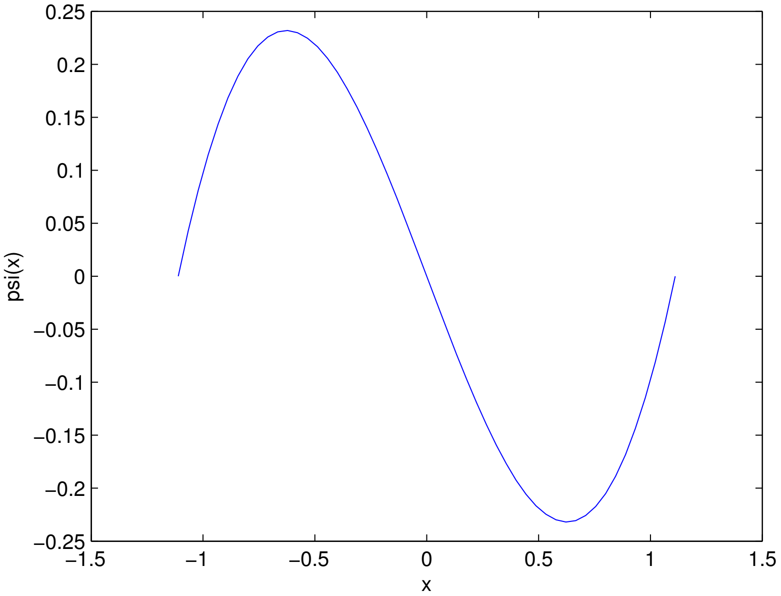

Figure 3.1 The eigenfunction associated with the smallest eigenvalue. Because this is a perturbation in terms of ψ, it is necessary to take a derivative in order to get the minimum eigenfunction for the governing equation in terms of ρ.

Next, we can rewrite the second order eigenvalue equation as the system

$$z_x = \left(2 - \frac{2\lambda}{\sqrt{2}M\cos(\sqrt{2}x)}\right)\tilde{\psi}, \tag{3.77}$$

$$\tilde{\psi}_x = z. \tag{3.78}$$

Using a fourth-order Runge-Kutta algorithm with shooting the eigenvalues can be computed numerically. The smallest eigenvalue is $\lambda = 2.37$. For the smallest eigenvalue, the associated eigenfunction is shown in Figure 3.1. This result shows what is expected from the energy based perturbation analysis. The solution converges to the steady-state for small perturbations both inside and outside the region of support.

Chapter 4

Extensions to Higher Dimensions

In this chapter I will present the analogous model for higher dimensions. Radially symmetric steady-state solutions for an interval $[a, b]$ are derived, however, none appear to be solutions to the problem in $\mathbb{R}^n$ and it is unclear if they are energy minimizers.

4.1 The Model in Higher Dimensions

For the attractive and repulsive forces used in the one-dimensional model, an analogous continuity equation exists for the model in higher dimensions. For a position vector $\vec{x}$, the continuity equation becomes

$$\rho_t(\vec{x}, t) + \nabla \cdot (\vec{V}(\vec{x}, t)\rho(\vec{x}, t)) = 0, \tag{4.1}$$

where

$$\vec{V}(\vec{x}, t) = \nabla Q(\vec{x}, t) - \nabla \rho(\vec{x}, t), \tag{4.2}$$

and

$$Q(\vec{x}, t) = |\vec{x}| * \rho(\vec{x}, t). \tag{4.3}$$

In order to attempt to find a steady-state solution, we assume it exhibits radial symmetry. This makes the equations tractable by allowing the replacement of $\rho(\vec{x}, t)$ with $\rho(r, t)$ and creating a set of equations that more closely resembles the one-dimensional case. Then Q becomes

$$Q(r, t) = \int_{S^N} d(r, r')\rho(r', t)d\Omega, \tag{4.4}$$

where $d\Omega$ is the volume element in $\mathbb{R}^N$, S^N is the N-sphere, and $d(r, r')$ is the Euclidean distance between two vectors in $\mathbb{R}^N$. By the law of cosines,

$$d(r, r')^2 = r^2 + r'^2 - 2rr' \cos(\phi), \tag{4.5}$$

where ϕ is the angle between the two radial vectors. By symmetry we can rewrite Q as

$$Q(r, t) = c_N \int_0^\infty \rho(r', t) r'^{N-1} \int_o^\pi \sqrt{r^2 + r'^2 - 2rr' \cos(\phi)} \sin^{N-2} \phi \, d\phi dr', \tag{4.6}$$

where c_N is the surface area of the unit sphere in $\mathbb{R}^{(N-1)}$. A more in depth discussion of a similar radially symmetric model can be found in Huang and Bertozzi (2010) along with a limited derivation of Q.

To find a steady-state solution we require that the velocity is zero in the support of the solution. Therefore to find the steady-state solution, it is sufficient to solve

$$V(r) = \nabla Q(r) - \nabla \rho(r) = \nabla(Q(r) - \rho(r)) = 0. \tag{4.7}$$

Integrating both sides,

$$Q(r) - \rho(r) = \lambda, \tag{4.8}$$

for some constant λ. Substituting in $Q(r)$ yields the integral equation

$$c_N \int_0^\infty \rho(r') r'^{N-1} \int_0^\pi \sqrt{r^2 + r'^2 - 2rr' \cos(\phi)} \sin^{N-2} \phi \, d\phi dr' - \rho(r) = \lambda. \tag{4.9}$$

For even powers of N the integral

$$k(r, r') = \int_0^\pi \sqrt{r^2 + r'^2 - 2rr' \cos(\phi)} \sin^{N-2} \phi \, d\phi \tag{4.10}$$

has elliptic equations as the solution. For odd powers of N, however, the integral evaluates to a solution in terms of powers r and r' along with signum functions. As a result, we now examine the $N = 3$ case as the next simplest model after $N = 1$. For $N = 3$, $k(r, r')$ simplifies to

$$k(r, r') = \begin{cases} \frac{2}{3} \frac{r'^2 + 3r^2}{r} & r' \leq r, \\ \frac{2}{3} \frac{3r'^2 + 2r^2}{r'} & r \leq r'. \end{cases} \tag{4.11}$$

The function $k(r, r')$ is continuous and differentiable. Assuming the solution has support $[a, b]$ where $a \geq 0$, then we can rewrite $Q(r)$ as

$$Q(r) = Q_1(r) + Q_2(r), \tag{4.12}$$

where

$$Q_1(r) = \int_a^r \frac{2}{3}\frac{\rho(r')r'^2(3r^2+r'^2)}{r}\,dr', \tag{4.13}$$

$$Q_2(r) = \int_r^b \frac{2}{3}\rho(r')r'(3r'^2+r^2)\,dr'. \tag{4.14}$$

In order to simplify taking derivatives of the integral equation we multiply both sides of the equation by r. This yields the modified integral equation

$$rQ(r) - r\rho(r) = r\lambda. \tag{4.15}$$

Differentiating four times with respect to r, the integral equation becomes the differential equation

$$4r\rho(r) + 4\frac{d^3}{dr^3}\rho(r) + r\frac{d^4}{dr^4}\rho(r). \tag{4.16}$$

The four solutions to the equations are in terms of elementary functions. The solutions are

$$S_1(r) = \frac{\sinh(r)\sin(r)}{r}, \tag{4.17}$$

$$S_2(r) = \frac{\cosh(r)\cos(r)}{r}, \tag{4.18}$$

$$S_3(r) = \frac{\cosh(r)\sin(r)}{r}, \tag{4.19}$$

$$S_4(r) = \frac{\sinh(r)\cos(r)}{r}. \tag{4.20}$$

Substituting the general solution of the differential equation given by

$$\rho(r) = A_1S_1(r) + A_2S_2(r) + A_3S_3(r) + A_4S_4(r), \tag{4.21}$$

creates a system of equations that yields a solution in terms of a and b, the edges of support.

4.2 Solution Intervals and Nonphysical Solutions

There are intervals $[a, b]$, primarily with a at or near zero and $b < 1$, that admit physical solutions where $\rho(r) \geq 0$ for $r \in [a, b]$. However, finding an interval where either $a = 0$ and $\rho(b) = 0$, or $\rho(a) = \rho(b) = 0$ proves to be more difficult. If a solution of this form exists it is possible it is a

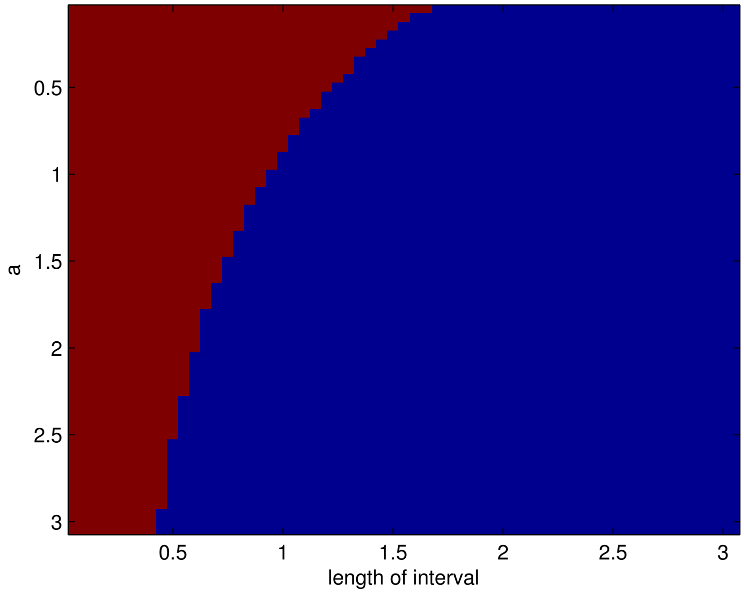

Figure 4.1 The red section of the graph represents choices of a and corresponding lengths of support where the steady-state solution has a physically realizable solution. Where the grid is blue there is some interval of the steady-state solution, possibly near one of the end points, where the density changes sign. This indicates that if a steady-state solution exists, it likely has finite support.

steady-state solution for the original partial differential equation when we allow $r \in \mathbb{R}^+$, while the other solutions are only steady-state solutions if the swarm is confined to the interval $[a, b]$ since it is likely the energy minimizer.

In addition, for the vast majority of the space of possible choices of a and b the steady-state solution includes sections where the density is less than zero. In Figure 4.1, the physical solutions appear to only occur for regions of finite support, particularly when b is not much greater than a.

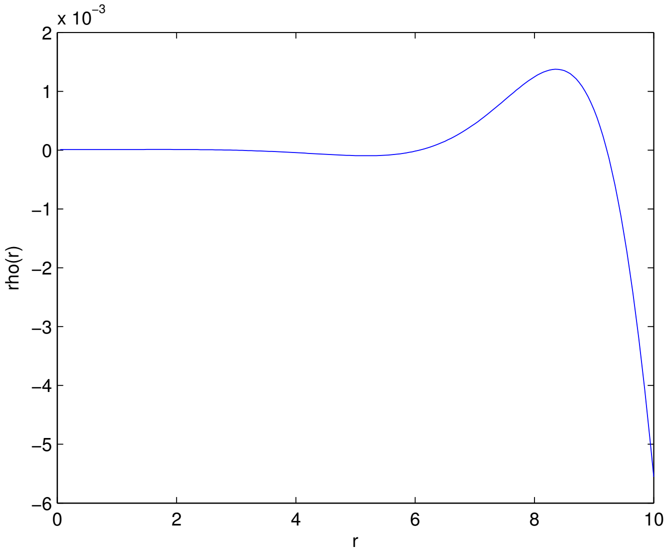

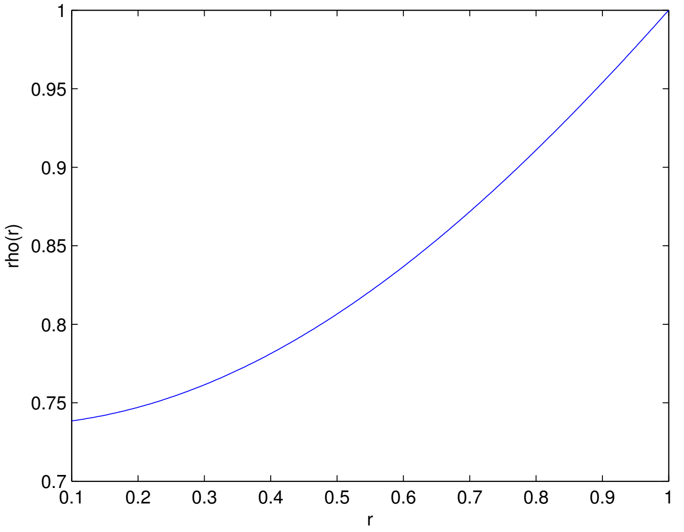

Figure 4.2 The first image shows the density distribution of a nonphysical steady-state solution. While there are components that are less than zero, the vast majority of the density appears to be concentrating toward the outer edge of the support. The second image shows the density distribution of the steady-state solution for the interval $[0.1, 1]$. Interestingly, the repulsive forces appear to be stronger than the attractive forces resulting in a higher swarm density at higher radii.

Chapter 5

Numerical Simulations

In this chapter I explain the Lagrangian approach used to model the swarm distribution numerically. In one dimension the results are shown to match closely with the analysis conducted in Chapter 3; however, for the higher-dimensional case the numerical results and the analytical results appear to disagree.

5.1 Derivation of the Model

In order to do numerical simulations to simulate the original continuous partial differential equation, we return to the discrete Lagrangian model introduced in Chapter 1. The cumulative mass function for the discrete model is

$$\psi_D(x_i) = i - 1/2, \tag{5.1}$$

where we have used the convention that integrating up to a δ-function yields half the mass of integrating through it. The velocity for a particle x_i is given by

$$\frac{dx_i}{dt} = V_a + V_r. \tag{5.2}$$

The signum function for the attractive velocity simplifies to

$$V_a = (n - 2k + 1)m \tag{5.3}$$

for a simulation with particles $x_1, \ldots, x_n$. The repulsive component remains the same,

$$V_r = -\psi_{xx}. \tag{5.4}$$

The second derivative of ψ is computed by numerical differentiation via three-point interpolation. Two additional phantom points are required, one on each end of the support, where the density is zero at the edge of the support in order to fulfill all the constraints on ψ. These additional points are incorporated into the numerical simulation because we require that $\psi_x = \rho = 0$ at these points. These constraints imply that $\psi(x_0) = 0$ and $\psi(x_{n+1}) = M$.

For comparison to the steady-state solution, the numerical solutions are normalized and translated so that the center of mass is the origin. In addition, the density ψ_x at the x_i points is computed via differentiation of a three-point interpolating polynomial.

5.2 Analysis

To accurately compute the error in the numerical simulation from the analytical solution, the solution is imposed on an equally spaced grid where the value of each point in the grid is computed via linear interpolation of the densities ρ_i of the original and additional phantom particles.

Trivially, the mass of the system is maintained at each time step. In addition, as expected the center of mass remains unchanged. As can be seen in Figure 5.1, initial conditions outside the support of the steady-state solution as well as those inside the domain of support converge to the steady-state solution. After rescaling the solution, there is strong agreement between the steady-state solution and the discrete simulation. The agreement can be seen in terms of both ρ and ψ in Figure 5.1. A refinement study using 40, 80, 120, and 160 particles indicates that in the limit as $n \to \infty$ the solution converges to the steady-state solution because the error approaches zero and does not appear to converge to a nonzero constant.

Define the L_2 error as

$$\epsilon = \sqrt{\int_{-\infty}^{\infty} |\rho - \bar{\rho}| \, dx}, \tag{5.5}$$

where ρ is the solution at time t and $\bar{\rho}$ is the steady-state solution. To implement the error numerically, we take the difference of the numerical solution imposed on the grid and the steady-state solution, square it, and then use the trapezoid rule to integrate over all the points in the grid. Examining the natural log of the L_2 error for a small perturbation from the steady-state solution indicates that the size of the L_2 error is given by

$$\epsilon = Ce^{-\lambda t}, \tag{5.6}$$

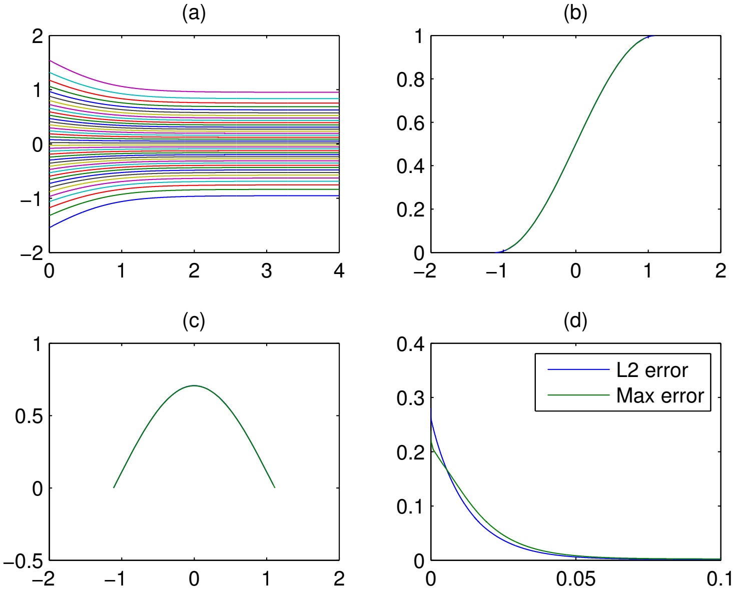

Figure 5.1 In (a), starting with a quintic density distribution of 40 particles with zeros outside the range of support of the steady-state solution the particles converge rapidly to a steady-state solution. In (b), the rescaled cumulative density function of the discrete particles is compared to the analytical solution while in (c) the solution is compared to the steady-state solution in terms of ρ. In (d), the maximum and L_2 error are computed for each time step. Both errors converge rapidly to a near zero constant.

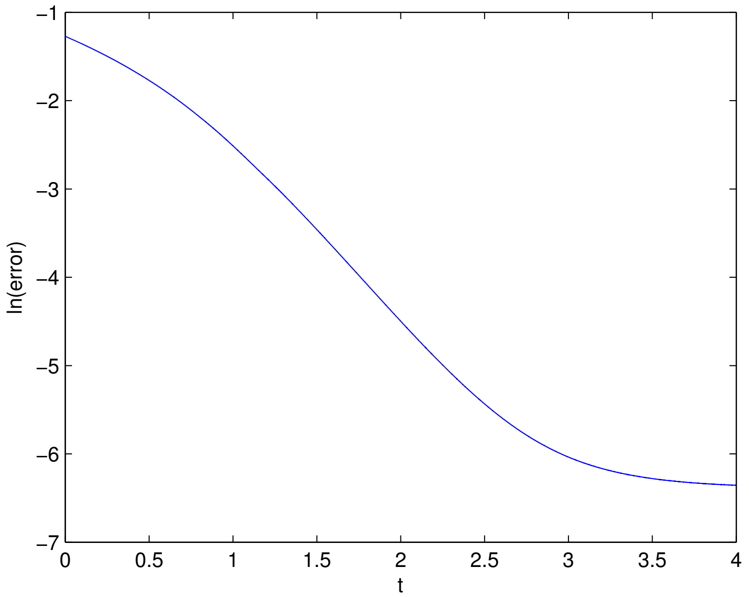

Figure 5.2 The natural log of the L_2 error for a small perturbation from the steady-state solution in time for 40 particles. After the initial decline, the point where numerical errors dominate is reached and the size of the error becomes constant in time. Taking a linear fit of the plot from 1.5 to 2.0 seconds, the plot has a slope of approximately -2.1, which corresponds to an minimum eigenvalue of 2.1.

where $-\lambda$ is the slope of the natural log of the L_2 error. For forty particles the slope of the natural log of the error is approximately -2.1. The slope corresponds to a minimum eigenvalue of 2.1, which is similar to the minimum eigenvalue of 2.37 found from linear perturbation theory. In addition, as the number of particles increases the value of the minimum eigenvalue appears to converge to 2.37. For example, for 100 particles the slope of the natural log of the L_2 error is -2.24.

In addition to examining the change in size of the L_2 error in time to determine the magnitude of the smallest eigenvalue, the shape of the error, or the perturbation after a small amount of time, should give an indication of what the eigenfunction corresponding to the smallest eigenvector looks like. For perturbations both inside and outside the region of support of the steady-state solution the error at each point resembles a cosine function seen in Figure 5.3. Rescaling the numerical error and the smallest eigen-

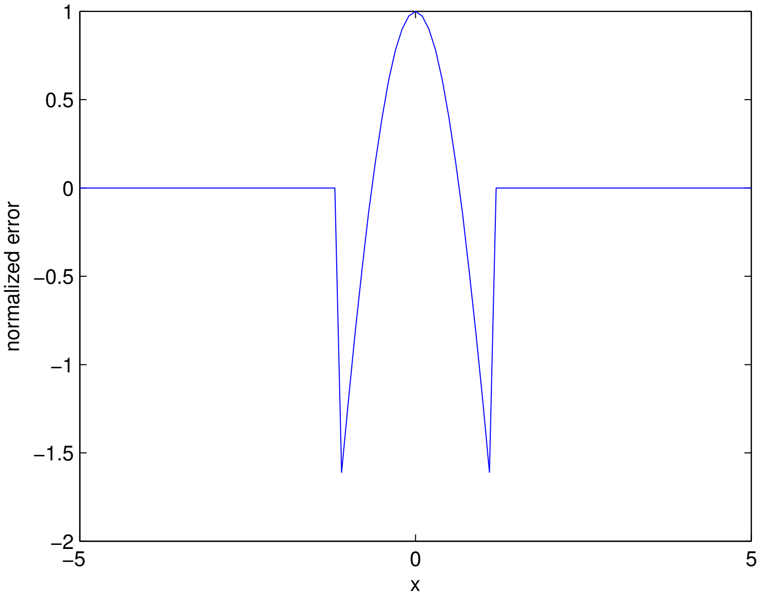

Figure 5.3 The normalized error at each particle from the steady-state solution. For all perturbations it quickly converges to this sinusoidal function indicating that the smallest eigenvalue has an associated eigenfunction that resembles a cosine.

value from the perturbation theory analysis, the two functions appear to be identical. This indicates that the numerical results closely resemble what was expected from linear perturbation theory.

5.3 Numerical Simulations in Higher Dimensions

Utilizing the same particle based approach as the one-dimensional model, we need to calculate the velocity of each individual particle. Recall from Chapter 3 that the velocity function is given by

$$V(r) = \nabla Q(r) - \nabla \rho(r), \tag{5.7}$$

where

$$Q(r,t) = c_N \int_0^\infty \rho(r',t) r'^{N-1} \int_o^\pi \sqrt{r^2 + r'^2 - 2rr' \cos(\phi)} \sin^{N-2}\phi \, d\phi dr'. \tag{5.8}$$

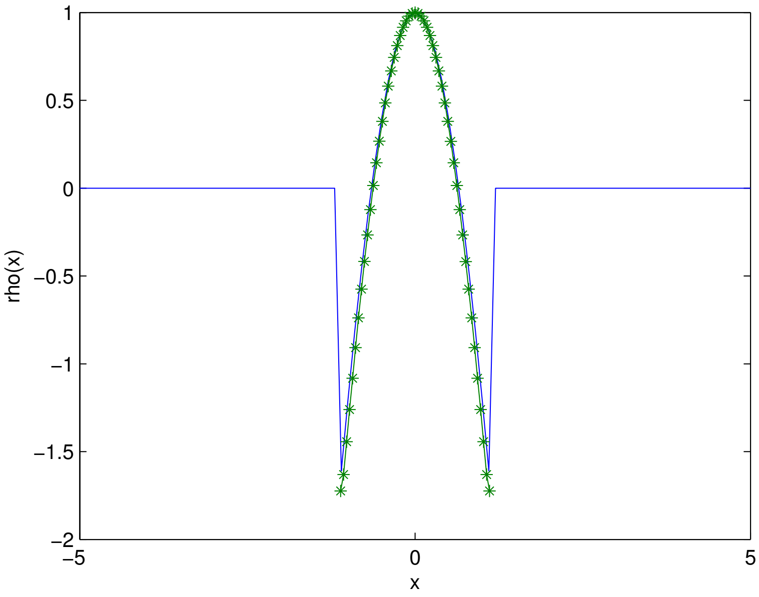

Figure 5.4 The normalized error from the particle simulation which should converge to the minimal eigenvalue is represented in blue. The green line represents the normalized derivative of the minimum eigenvalue from linear perturbation analysis since the analysis was done in terms of the cumulative density function, $\psi(x)$.

By radial symmetry,

$$V(r) = Q_r(r) - \rho_r(r). \tag{5.9}$$

Substituting in the expression for $Q(r)$,

$$V(r) = c_N \int_0^\infty r'^2 \rho(r') k_r(r, r') dr' - \rho_r(r). \tag{5.10}$$

While $k(r, r')$ is differentiable with respect to r, the density at our particles, or in this case concentric spheres, is proportional to the radius. To simplify the numerics, let $m(r)$ be the mass of the shell of radius r. Then,

$$m(r) = 4\pi r^2 \rho(r). \tag{5.11}$$

Substituting mass in the place of density in the velocity function and applying the chain rule we have

$$V(r) = c_N \int_0^\infty m(r') k_r(r, r') dr' - \frac{m_r(r)}{4\pi r^2} + \frac{2m(r)}{4\pi r^2}. \tag{5.12}$$

Using a three-point interpolation to calculate the derivative of $m(r)$, we can discretize the velocity function as

$$V_i = c_N \sum_{i=1}^{n} m_i k_r(r, r') - \frac{m_r(r)}{4\pi r^2} + \frac{2m(r)}{4\pi r^2}, \tag{5.13}$$

where m_i is the ith concentric shell of mass m_i.

As seen in Figure 5.5, the numerics indicate that the steady-state solution has the majority of the mass of the swarm near the origin where $r = 0$. It is possible that the swarm is converging to a δ-function, though some of the shells do appear to be steady away from zero. The posititions of the mass shells indicates that it is possible the solution blows up at $r = 0$. Unfortunately, doing a nonlinear least squares fit of the four solutions derived in Chapter 4 with the solution does not produce a good fit. In addition to the poor fit with the analytical solutions, the numerical results appear contrary to the steady-state solutions found in Chapter 4 where the mass appeared to be concentrating at the outside edge of the support. It is possible there is an error in the numerics resulting in the distribution seen in Figure 5.5, or that perhaps the finite number of shells is not capturing the behavior accurately. Either way, the numerical results appear to contradict the analytical results.

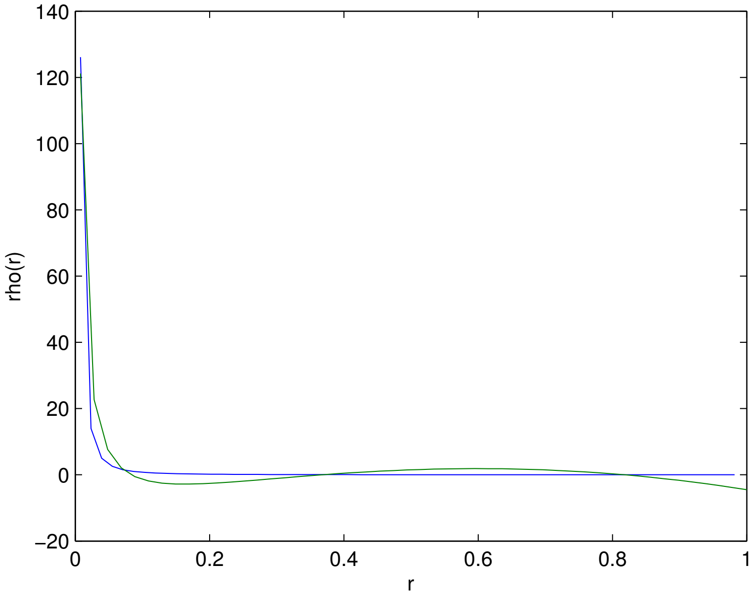

Figure 5.5 The blue line represents the density of the swarm at each of the particle points. The green function is the least squares fit of the four analytical solutions to the numerical data. The poor fit potentially indicates problems with the numerics.

Chapter 6

Conclusions and Future Work

In one dimension, the numerical results agree strongly with the results from the perturbation theory. The solution appears to converge to the steady-state globally. The size of the minimum eigenvalue being larger than one may indicate why looking at the sinusoidal solutions to the energy minimization eigenproblem did not provide any eigenfunctions that met all the physical constraints. Perhaps by incorporating the exponential solutions it maybe possible to find a minimum eigenvalue utilizing the Rayleigh quotient method, but it is unclear if it is even a finite sum of the solutions to the eigenproblem.

In addition to proving global convergence to the steady-state solution in one dimension, it seems possible to show well-posedness or at least existence of solutions for all time in a similar vein to the work that Bedrossian, Rodriguez, and Bertozzi did in their 2010 paper or Bertozzi and Slepcev did in their 2010 paper. While the behavior of the solution in the one-dimensional case appears to be well understood for any initial swarm distribution, the initial results from the three-dimensional case is far less clear.

The numerical results for the three dimensional case appear to show that the density distribution has finite support and blows up at $r = 0$. This is a similar result to the one-dimensional case since it has finite support, however now the solution also has a point at which the density blows up. It is also possible that the numerical results are actually pointing to a δ-function solution since the magnitude of the slope of the density near the origin is far larger than what a linear combination of the analytical solutions suggests. Additional research could be completed to determine how the energy of a δ-function compares with that of other density distributions including the steady-state distributions that occur along the border of the regions in Figure 4.1. There is a great deal of work remaining in the n-dimensional cases. While for even n the eigenvalue problem becomes significantly more complex, for odd values of n and especially for $n = 3$ it should be possible to find a steady-state solution without having to limit the region of the solution. A final possibility is that the assumption of radial symmetry is not correct and that there is not a radially symmetric steady-state solution.

Bibliography

Bedrossian, Jacob, Nancy Rodriguez, and Andrea Bertozzi. 2010. Local and global well-posedness for aggregation equations and Patlak-Keller-Segel models with degenerate diffusion. Unpublished.

Bernoff, Andrew J., and Chad M. Topaz. 2010. A primer of swarm equilibria. Preprint.

Bertozzi, Andrea L., and Dejan Slepcev. 2010. Existence and uniqueness of solutions to an aggregation equation with degenerate diffusion. *Communications on Pure and Applied Analysis* 9(6):1617–1637.

Bodnar, Marek, and Juan J.L. Velazquez. 2005. Derivation of macroscopic equations for individual cell-based models: A formal approach. *Mathematical Methods in the Applied Sciences* 28(15):1757–1779.

———. 2006. An integro-differential equation arising as a limit of individual cell-based models. *Journal of Differential Equations* 222(2):341–380.

Brecht, James von, David Uminsky, Theodore Kolokolnikov, and Andrea Bertozzi. 2011. Predicting patterns that arise in N-dimensional particle interactions. Preprint.

Huang, Yanghong, and Andrea Bertozzi. 2010. Self-similar blowup solutions to an aggregation equation in RN. *SIAM Journal of Applied Mathematics* 70(7):2582–2603.

Leverentz, Andrew J. 2008. An integrodifferential equation modeling 1-D swarming behavior. Harvey Mudd College Mathematics Senior Thesis.

Leverentz, Andrew J., Chad M. Topaz, and Andrew J. Bernoff. 2009. Asymptotic dynamics of attractive-repulsive swarms. *SIAM Journal on Applied Dynamical Systems* 8(3):880–908.

Mogilner, Alex, Leah Edelstein-Keshet, Leeann Bent, and Athan Spiros. 2003. Mutual interactions, potentials, and individual distance in a social aggregation. *Journal of Mathematical Biology* 47(4):353–389.